ACS OMEGA

Article

Cite This: ACS Omega 2020, 5, 219−227

http://pubs.acs.org/journal/acsodf

Interfacially Interactive Ternary Silver-Supported Polyaniline/Multiwalled Carbon Nanotube Nanocomposites for Catalytic and Antibacterial Activity

Shamkumar P. Deshmukh,[†,‡] Ananta G. Dhodamani,[†] Satish M. Patil,[†,§] Sajid B. Mullani,[†] Krantiveer V. More,[†] and Sagar D. Delekar*[,†]

[†]Department of Chemistry, Shivaji University, Kolhapur 416 001, Maharashtra, India

[‡]Department of Chemistry, D. B. F. Dayanand College of Arts and Science, Solapur 413 001, Maharashtra, India

[§]Department of Chemistry, Karmaveer Hire Arts, Science, Commerce and Education College, Gargoti, Kolhapur 416 209, Maharashtra, India

Supporting Information

ABSTRACT: Herein, a protocol strategy has been designed for the preparation of ternary silver nanoparticles-supported polyaniline multiwalled carbon nanotube (Ag NPs−PANI/MWCNT) nanocomposites with a chemical interaction for catalytic and antibacterial activity. The morphological study confirmed that Ag NPs were immobilized on the surface of PANI, and afterward, Ag NPs−PANI were mixed with the MWCNTs. The X-ray diffraction technique revealed the face-centered cubic structure of Ag NPs, and the X-ray photoelectron spectroscopy study revealed the chemical constituent and signature of $\pi-\pi^*$ and C−N interactions in the nanocomposites. The ternary Ag NPs−PANI/MWCNTs nanocomposites have the apparent rate of reaction (K_{app}) as 5.4×10^{-3} s^{-1}, higher than binary nanocomposites for catalytic reduction of 4-nitrophenol to 4-aminophenol at room temperature. Antibacterial activity of Ag NPs−PANI/MWCNT nanocomposites is higher against pathogenic bacteria. Thereafter, because of multifold applications of ternary nanocomposites, they have a broad scope in the field of environmental and healthcare sectors.

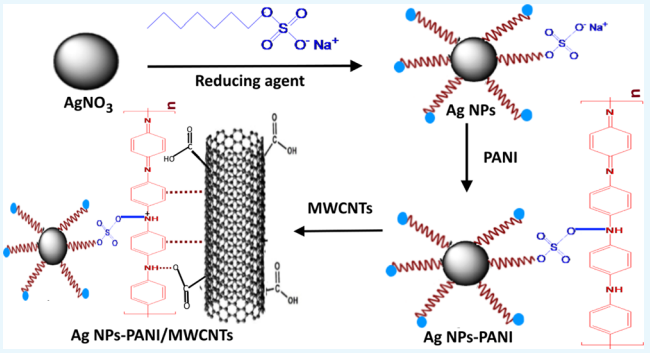

1. INTRODUCTION

In recent times, energy exploitation, environmental remediation, and multiresistance bacteria have attracted extensive concern globally. Hence, investigators are continuously trying their level best with the search of smart materials for a wide variety of applications.[1] Noble metal Ag nanoparticles (NPs) are potential candidates used commonly in catalysis, antibacterials, and sensors because of their excellent optical, catalytic, and antimicrobial properties which depend on size, shape, composition, and structures.[2,3] Particularly, Ag NPs have a tendency to aggregate because of high surface energy and subsequently lose their catalytic activity. Therefore, to enhance properties as well as stability, there is a need to make its composites with other. To conquer these problems, Ag NPs are incorporated into solid supports such as metal oxides,[4] polymers,[5] carbonous materials,[6] and biomaterials.[7] Among the various supportive materials, conducting polymer is most suitable material because it owes intermolecular interaction to upgrade optical and electrical properties resulting in the effective use into enzymatic and nonenzymatic sensors, actuators capacitors, catalysis, electronic devices, fuel cells.[8,9] Polyaniline (PANI) is one of the cheapest, easily accessible, environmentally stable, easily separable, and best supporting polymer material which is insoluble in organic solvents.[10] In addition, the PANI polymer has been enhancing the rate of the host materials for catalytic and antibacterial activity. Shaban et al. reported the nanoporous Ag NPs−PANI nanocomposite prepared by using the oxidation route and utilized it as an antibacterial agent.[11] The silver−PANI (Ag NPs−PANI) nanocomposite synthesis protocol is time-consuming, and it shows antibacterial activity against the only *B. substilis* pathogenic bacteria.[12] Heterogeneous (Ag NPs−PANI) nanocomposites were prepared with an optimized morphology using a higher pressure and temperature method, which was a tedious process.[13] Sophisticated instruments are used for the preparation of the nanocomposite, but a microscopic study revealed that silver is not well distributed on the surface of the PANI nanocomposites.[14] However, the efficiency of Ag NPs−PANI in the various applications is not up to the mark, and hence, it is necessary to modify the Ag NPs−PANI for further

Received: August 7, 2019
Accepted: November 1, 2019
Published: December 26, 2019

DOI: 10.1021/acsomega.9b02526
ACS Omega 2020, 5, 219−227

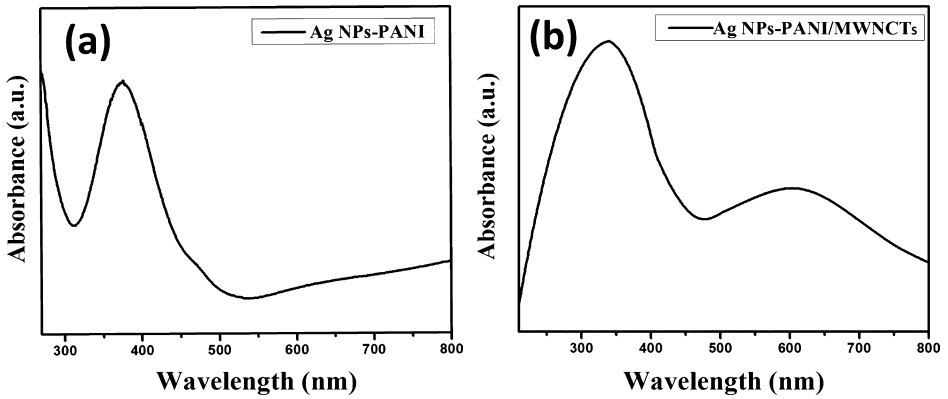

Figure 1. UV−visible spectra of (a) Ag NPs−PANI and (b) Ag NPs−PANI/MWCNTs.

research endeavors. Nowadays, carbon-based materials such as graphene, activated carbon, and carbon nanotubes (CNTs) have been used in the areas of the fuel cells, sensors, catalysis, and capacitors. Among the various carbon nanostructures, CNTs are a promising candidate for hybrid nanocomposites because of their large surface area, incredible electronic characteristics, and good structural and mechanical properties.[15] The nanofibrous structures of CNTs have excellent cell adherence and efficient electrostatic interaction with the cell membrane compared to other structures. In addition, generations of reactive oxygen species have affected biological molecules and led to DNA destruction. The insertion of impurities in multiwalled CNTs (MWCNTs) possesses optimized antibacterial activities. One-dimensional CNTs and zero-dimensional Ag NPs can also promote the antibacterial as well as catalytic activity.[16] Wen et al. reported that a polyacrylonitrile PANI silver nanowires−carbon fiber cloth composite membrane filter is a better disinfectant.[17] Hybrid PANI/graphene/CNT nanocomposites are used in water disinfection, but the overall synthesis protocol is tedious.[18] Zhang et al. reported that carbon nanofibers/Ag NPs efficiently reduce 4-nitrophenol (4-NP) because of the high surface area and electron transfer between CNFs and Ag NPs.[19] Though uniform distribution, adsorption capability and electron migration of graphene to silver results the effective catalyst for reduction of 4-NP, however a rate constant for the said conversion is not up to the mark than others.[20] In addition, the optimized synthetic protocol of Fe_3O_4@SiO_2@Au−PANI is complicated, even though it reduces the aggregation of silica particles and is employed for the catalytic activity.[21] Micro- and nanostructured PANI−Ag composites have been prepared using nitric acid which is employed for the catalytic study, but the use of acid is not an environmentally benign method.[22] However, the individual metals, polymers, as well as carbon-based materials due to their unique properties are used in various applications individually, but the major challenge is to tailor their properties successfully for antibacterial as well as catalysis application. In consequence of that, there is an urgency to design materials with low-cost preparation and synergistic properties of all individual elements for both applications. The synergy of these materials would result in the enhanced properties of individual bare materials. The ternary Ag NP−PANI/MWCNT composite has been designed by the wet chemical method, and it is used for its catalytic and antibacterial activity. To the best of our knowledge, the optical, structural, catalytic, as well as antibacterial properties of Ag NPs−PANI/MWCNT composite are obscure.

2. RESULTS AND DISCUSSION

2.1. UV−Visible Spectroscopy. The absorption peak at 270 nm is attributed to F-MWCNTs as shown in Figure S1a. For PANI, the absorption bands are found at 566 nm which are attributed to the $\pi-\pi^*$ transition due to the quinonoid, as shown in Figure S1b. Ag NPs−PANI showed a broad absorption band at 375 nm, which signifies a surface plasmon resonance band of Ag NPs because of the absorption of an electron from the conduction band of silver as shown in Figure 1a.[23] The absorption band of Ag NPs−PANI/MWCNTs showed two distinct peaks at 340 and 600 nm, as shown in Figure 1b. The longer shift of the peak is observed from 331 to 370 nm because of the presence of silver nanoparticles in binary nanocomposites. Furthermore, the peaks observed are shifted from 331 to 340 nm because of the presence of silver and CNT reduction of slight shift of the absorption peak of the benzonoid ring.[24]

2.2. Fourier Transform Infrared Spectroscopy. Figure 2b shows Fourier transform infrared (FTIR) spectra of pure

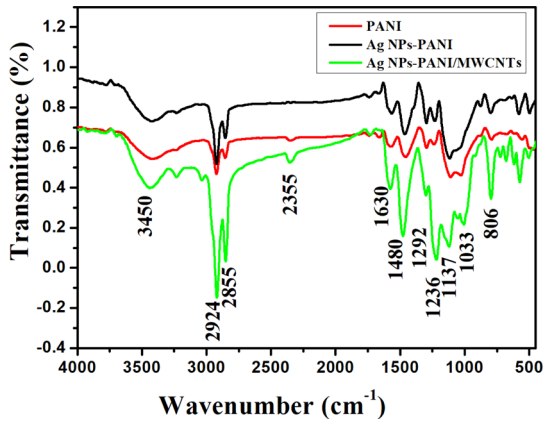

Figure 2. FTIR spectra of PANI, Ag NPs−PANI, and Ag NPs−PANI/MWCNTs.

PANI, Ag NPs−PANI, and Ag NPs−PANI/MWCNT nanocomposites. The characteristic peak of pure PANI is at 1480 and 1630 cm^{-1} of C=C stretching of benzenoid and quinonoid rings, respectively. Particular bands are observed at 1292 and 1236 cm^{-1} which represent C−N stretching of benzenoid and quinonoid rings. In addition, bands found at 2924 and 2855 cm^{-1} indicated hydrogen bonding, and two benzene nuclei shown at 2355 cm^{-1} and out-of-plane bending C−H vibration at 806 cm^{-1} was observed because of the *p*-

DOI: 10.1021/acsomega.9b02526
ACS Omega 2020, 5, 219−227

substituted benzene ring.[25] The distinctive band centered at 668 cm^{-1} corresponds to the C−S stretching of the benzenoid ring of *para*-toluene sulphonic acid (*p*-TSA). The peak of the N−H vibration has been shifted from 3450 to 3420 cm^{-1}. This red shift is the significance of the conjugated electron cloud among Ag NPs and PANI and MWCNT chains.[26] The specific peak at 1137 cm^{-1} with an increase in intensity indicates the N═Q═N band which has a strong interaction between the quinoid ring of PANI and the π-bonded outer part of the MWCNTs.[27] In the Ag NPs−PANI/MWCNT nanocomposites, a specific peak at 1033 cm^{-1} interprets the interaction of silver with PANI along with additional bands that were observed to be similar to bare PANI. Structural features of the PANI show that their surface structure is not affected after formation of the nanocomposites.[28]

2.3. X-ray Diffraction Analysis. X-ray diffraction (XRD) patterns of Ag NPs−PANI and Ag NPs−PANI/MWCNT nanocomposites are determined for structural properties of the polymer in the composites, which are depicted in Figure 3. The

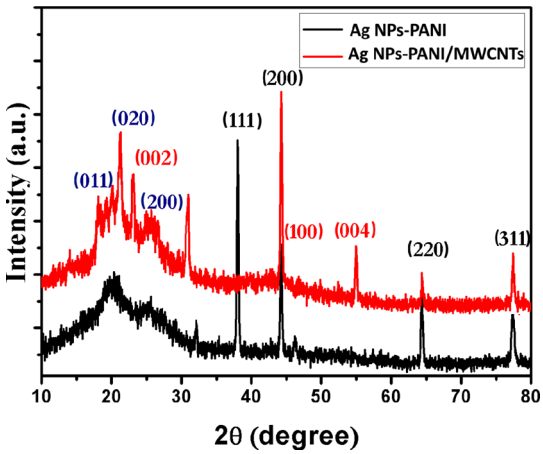

Figure 3. XRD pattern of Ag NPs−PANI and Ag NPs−PANI/MWCNTs.

XRD pattern of PANI showed a broad hump at 2θ = 15.16, 19.50, and 25.16° which corresponds to the (011), (020), and (200) crystal planes of emeraldine salt of PANI, respectively, as shown in Figure S2.[29] In the Ag NPs−PANI, the characteristic peaks of silver at 38.25, 44.42, 64.55, and 77.49°, are assigned to phase (111), (200), (220), and (311) reflections, respectively, with (JCPDS 4-0783) and (011), (020), and (200) crystal planes of emeraldine salt of PANI observed.[30] In the Ag NPs−PANI/MWCNTs, the peaks at 2θ = 25.2, 43.2, and 53.7° correspond to (002), (100), and (004); all these peaks indicate the diffraction pattern between the interplanar spacing of MWCNTs along with the reflection plane of Ag NPs and emeraldine salt of PANI observed.[31] The XRD results exhibit that Ag NPs−PANI and Ag NPs−PANI/MWCNTs are more crystalline in nature than PANI because of crystalline Ag NPs in the composites. The crystallite size of Ag NPs was calculated using the Scherrer's formula

$$D = \kappa\lambda/\beta \cos\theta$$

where κ is the shape factor and has a value of 0.9, λ is the wavelength (Cu Kα = 0.15405 nm), β is the full width at half maximum of the most intense peak (in radians), and θ is the peak position. The average crystalline sizes of Ag NPs in the nanocomposites are observed to be at ∼15 nm.

2.4. TEM Analysis. Figure 4 shows the representative transmission electron microscopy (TEM) micrograph of Ag

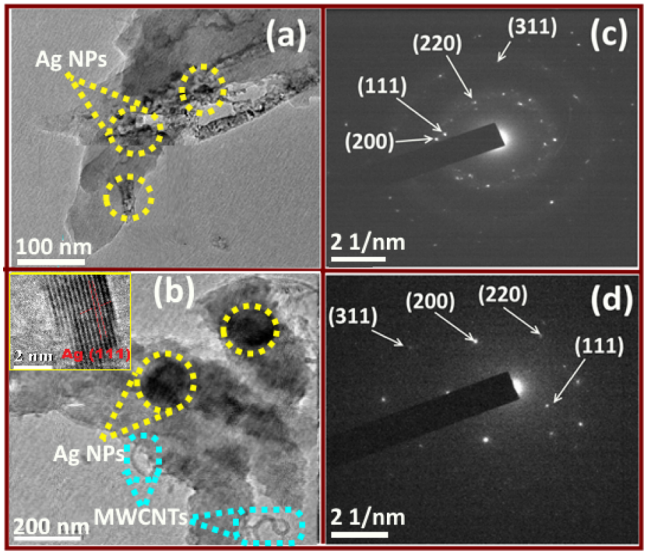

Figure 4. TEM images of (a) Ag NPs−PANI, (c) SAED of Ag NPs−PANI, (b) Ag NPs−PANI/MWCNTs, and (d) SAED of Ag NPs−PANI/MWCNTs.

NPs−PANI and Ag NPs−PANI/MWCNTs. Figure S3a represents the cylindrical tube of F-MWCNTs with an average diameter of 20−30 nm. PANI has also displayed a 15 nm particle size distribution as shown in Figure S3b. As shown in Figure 4a, the TEM image shows the blackish dark spot of Ag NPs that were observed on the surface of PANI with an average particle size of 10−14 nm. Figure 4c,d exhibits the selected area diffraction pattern of Ag NPs−PANI and Ag NPs−PANI/MWCNTs, respectively. Figure 4b exhibits Ag NPs−PANI/MWCNTs as a small dark spot of silver which also indicates the good distribution, particularly on the surface, and their histogram represents particle size distribution for Ag within the range of 15−20 nm. The distribution of Ag nanoparticles occurs along with the π−π* interaction between MWCNTs and aniline monomers; additionally, hydrogen bonding within the carboxyl groups of MWCNTs and amino groups of aniline monomers also takes place.[32] However, the inset picture of high-resolution TEM (HRTEM) indicates that distinct lattice fringes with a *d* spacing of 0.42 nm corresponds to the (111) lattice planes of the fcc of silver. Compared to Figure S3b, we can visualize from Figure 4a,b that all Ag NPs are successfully anchored on PANI and PANI/MWCNTs. The SAED pattern depicted in Figure 4c,d has diffraction ring (111), (200), (220), and (311) reflection planes of silver. According to the results obtained, they exhibit the crystalline nature of nanocomposites using HRTEM and SAED patterns, which are also in concordance with the XRD diffraction pattern. Figure S3c,d represents the particle size histogram of Ag NPs−PANI and Ag NPs−PANI/MWNCTs. Scanning electron microscopy micrographs of (a) Ag NPs−PANI and (b) Ag NPs−PANI/MWNCTs are depicted in Figure S4. It specifies that lumps of particles with uniform aggregation of polymer composites and the clouded matter signify the stable composite morphology.

2.5. Raman Analysis. Raman spectroscopy is used to analyze the interaction of Ag NPs−PANI and Ag NPs−PANI/

DOI: 10.1021/acsomega.9b02526
ACS Omega 2020, 5, 219−227

MWCNTs shown in Figure 5. Raman spectra of PANI, shown in Figure S5, exhibit peaks at 1360, 1494, 1598, and 1170 cm^{-1}

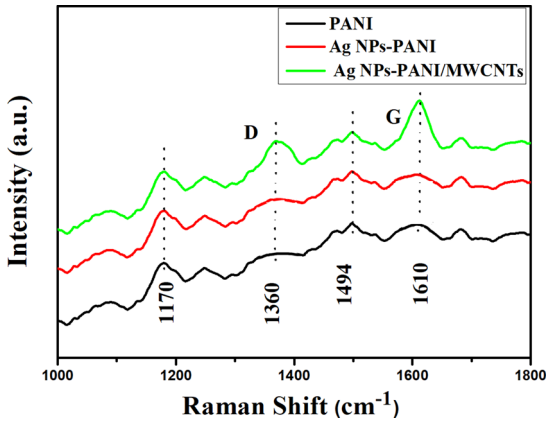

Figure 5. Raman spectra of Ag NPs−PANI and Ag NPs−PANI/MWCNTs.

which are assigned to C−N^+ stretching, C═N structure, C−C stretching of the quinonoid group, and C−H bending of the benzenoid structure, respectively. Similar bands are observed in Ag NPs−PANI, but the bands at 1360 and 1170 cm^{-1} have shifted to 1343 and 1179 cm^{-1}, which indicates the interaction between Ag and PANI.[33] Afterward, Ag NPs−PANI/MWCNT nanocomposites are ascribed to the D band at 1325 cm^{-1} and to the G band at 1578 cm^{-1} of MWCNTs. The shifting of D and G bands exhibits a little defect in the MWCNTs due to being embedded in the polymer.[34] On the other hand, peaks of carboxylated MWCNTs have been overlapped with PANI peaks and exhibit a strong interaction between MWCNTs and PANI.

2.6. XPS Analysis. X-ray photoelectron spectroscopy (XPS) spectra depicted the bond structure and its chemical status of the samples. Survey spectra of Ag NPs−PANI/MWCNTs consisting of C, O, N, and Ag elements are shown in Figure 6a. Nitrogen and carbon elements were observed because of the amine group and MWCNTs present in the sample, respectively. The Ag 3d spectrum of two peaks of Ag $3d_{5/2}$ and Ag $3d_{3/2}$ at 367.9 and 373.5 eV is shown in Figure 6b, respectively. These peaks have a binding energy lower than that of bulk Ag such as Ag, that is, 368.6 eV for Ag $3d_{5/2}$ and 374.3 eV for Ag $3d_{5/2}$. The difference in binding energy between the characterstic peaks (5.6 eV) recording the presence of elemental Ag in the NCs. It also indicates that there is the interaction between Ag and PANI.[35] Deconvoluted peaks of N 1s are shown in Figure 6c, which have binding energies of 398.7, 399.8, 401.6, 402.8, and 403.9 eV. The peak at 398.7 eV having lowest binding energy exhibits (═N−) the immine group, and the peak at 399.8 eV revealed the nitrogen atom (−NH) of the amine group.[36] The peaks at 401.6 and 402.8 eV are assigned to a cationic nitrogen atom of the polymer backbone of the PANI. In addition, the combined peak of MWCNT/PANI composites has the higher binding energy (403.9 eV) than that of pure PANI, and it also has the signature of the carbon and nitrogen interaction.[37] Bonding interaction can be identified by deconvoluting C 1s peaks, as shown in Figure 6d, which is composed of sub-peaks assigned at about 284.1 (C−C), 285.2 (C−N), and 286.1 (C−N). In addition, the peak obtained at 286.2 eV was recognized as the $\pi-\pi^*$ "shake-up" satellite.[38]

2.7. Catalytic Studies. Among the various harmful pollutants, 4-NP is a severe pollutant; therefore, there is an urgent need to convert such harmful pollutants into a less hazardous compound for the purpose of a clean and safe environment and use for chemical application. In this context,

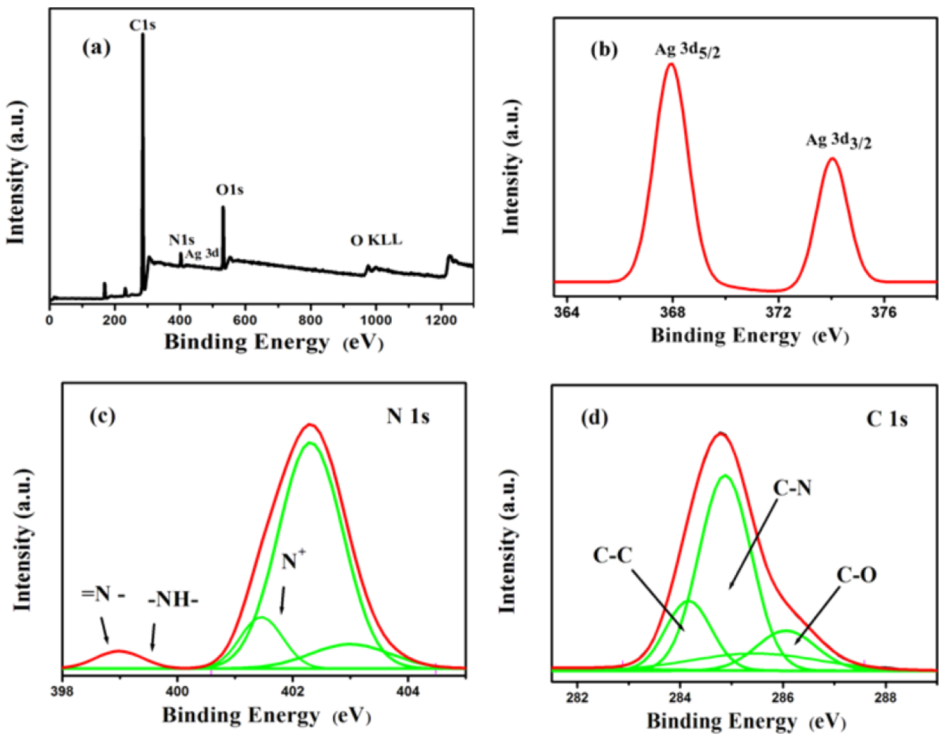

Figure 6. XPS spectra of the Ag NPs−PANI/MWCNTs: (a) survey, (b) Ag 3d, (c) N 1s, and (d) C 1s.

DOI: 10.1021/acsomega.9b02526
ACS Omega 2020, 5, 219−227

4-NP is reduced into 4-aminophenol (4-AP) as a product which is an effective reaction intermediate for the preparation of analgesic and antipyretic drugs and corrosion determent. Hence, the reduction of 4-NP to 4-AP has been taken as a model reaction for the study of the catalytic activity of Ag NPs−PANI/MWCNT and Ag NPs−PANI nanocomposites. The reduction of 4-NP cannot take place in the absence of a catalyst, even though an excessive amount of $NaBH_4$ is used. Particularly, the absorption peak of the 4-NP solution is depicted at 317 nm in neutral or acidic conditions, but the aqueous solution of $NaBH_4$ was added, and it strangely red-shifted to 400 nm because of the formation of 4-nitrophenolate ions.[39] Actually, the reduction reaction does not proceed in the absence of Ag NPs−PANI/MWCNT nanocomposites because of the greater kinetic barrier between nitrophenolate anions and BH_4^- ions and the unchanged absorption peak at 400 nm after 24 h. The catalyst is playing a vital role for the reduction of 4-NP in the presence of excess $NaBH_4$ and formation of the product with the new peak of 4-AP. Because of the addition of the catalyst, the decreases in absorption peaks at 400 nm indicate that the reduction process has started, as shown in Figure 7a; subsequently, the formation of a new characteristic peak at 300 nm made it clear the signature of the absorption peak of 4-AP.[40] As a consequence, it confirmed that the formation of 4-AP and complete conversion take place within 240 s. The complete disappearance of the yellow color of 4-nitrophenolate ion has resulted in the end of the reduction reaction. In addition, Figure 7b shows complete reduction of 4-NP to 4-AP within 300 s in the presence of Ag NPs−PANI as the catalyst. Herein, the time period required for the reduction of Ag NPs−PANI/MWCNTs is less than that of the Ag NPs−PANI catalyst. The excess amount of $NaBH_4$ in the reaction is taken into consideration for the reduction of 4-NP as a pseudo-first-order reaction. It is a linear relationship between $\ln(C_t/C_0)$ and the reaction time for the model reaction, in which C_t and C_0 are the concentrations of 4-NP at time t and 0, respectively. The apparent rates of reaction (K_{app}) determined from the liner plots are calculated as $K_1 = 5.4 \times 10^{-3}$ s^{-1} and $K_2 = 3.9 \times 10^{-3}$ s^{-1} for Ag NPs−PANI/MWCNTs and Ag NPs−PANI, respectively. These results exhibit that Ag NPs−PANI/MWCNTs have higher catalytic activity than Ag NPs−PANI because of the supports of PANI, and MWCNTs have a major role in the catalytic activity. For the further study, the activity factors are also determined for the performance of the catalyst. Then, activity factor κ (the ratio of K_{app} to the total weight of the catalyst) is calculated to be 5.40 and 3.9 s^{-1} g^{-1} for Ag NPs−PANI/MWCNTs and Ag NPs−PANI, respectively, which is greater than the nanocomposites reported in the literature.[22,41]

Catalyst have shown efficient activity because of the generation of active hydrogen atoms from sodium borohydride and these are adsorbed to Ag NPs−PANI/MWCNTs nanocomposites. Therefore, the active 4-NP hydrogen atoms are affecting to $-NO_2$ group of 4-NP to produce via −NO and −NHOH based intermediates. This Ag NPs−PANI/MWCNT can be considered as a definite prototype model for the migration of hydrogen ions from the sodium borohydride through a startup reduction process. The kinetics of the reaction is monitored when the reactant is adsorbed on the surface before starting the reaction by using the Langmuir−Hinshelwood mechanism.[42] The rate-determining step is executed because of adsorbed species in the reaction. The adsorption/desorption equilibrium is supposed to be much faster. Catalysts have shown better activity because of the following two reasons: first, electron transfer from PANI and

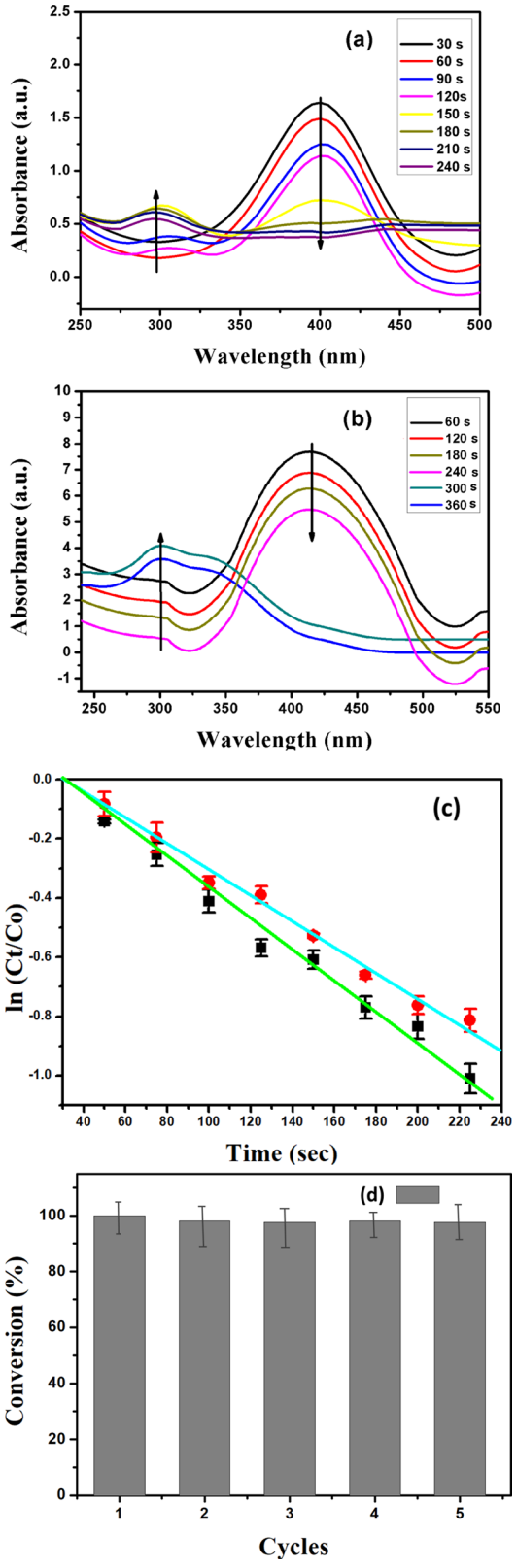

Figure 7. (a) UV−vis absorption spectra of reduction of 4-NP to 4-AP using Ag NPs−PANI/MWCNTs and (b) Ag NPs−PANI alone; conditions: [4-NP] = 1×10^{-4} M; [$NaBH_4$] = 0.1 M; catalyst = 1 mg. (c) Plot of $\ln(C_t/C_0)$ of 4-NP against time for the catalysts and (d) reusability of catalyst PANI/MWCNTs for reduction 4-NP.

DOI: 10.1021/acsomega.9b02526
ACS Omega 2020, 5, 219−227

Table 1. Zone of Inhibition Measured by the Disc Diffusion Method

	zone of inhibition in mm			
	bacteria			
	E. coli		*S. aureus*	
catalyst	10 μg/mL	20 μg/mL	10 μg/mL	20 μg/mL
Ag NPs	3	5	3	6
Ag NPs−PANI	7	10	8	9
Ag NPs−PANI/MWCNTS	17	20	16	19
streptomycin	20			
penicillin	22			

MWCNTs, which have a conducting nature, toward the silver nanoparticles enhances the catalytic activity.[43] Second, the strong $\pi-\pi$ stacking interactions of 4-NP and PANI along with MWCNTs lead to adsorption of 4-NP on its surfaces.[44] Increase in the interfacial contact due to maximum adsorption of the catalyst on the reactant boosts catalytic activity. In summary, the effective interactions between the PANI, MWCNTs, and Ag NPs and specific structural characteristic of Ag NPs−PANI/MWCNT nanocomposites induce the catalytic activity of the supported Ag NPs.

In the heterogeneous catalyst, reusability is the key advantage over the homogeneous catalyst. Hence, recyclability of Ag NPs−PANI/MWCNT nanocomposites was determined by repeating the model reaction up to five cycles as shown in Figure 7d. In each cycle, the catalyst was recovered and used as it is for the next cycle. It showed that up to five cycles was efficient for the reduction of 4-NP to 4-AP. In conclusion, such ternary nanocomposites are efficient for the reduction of an organic pollutant into the intermediate compounds for various applications.

2.8. Antibacterial Study of Ag NPs−PANI and Ag NPs−PANI/MWCNT Nanocomposites. As is well known, metallic silver and Ag NPs are the effective bactericidal agents.[45] In the present context, the antibacterial activity of Ag NPs, Ag NPs−PANI, and Ag NPs−PANI/MWCNT nanocomposites was studied with Gram-positive *S. aureus* and Gram-negative *E. coli* bacteria at various concentrations. We performed the experiment by the disc diffusion method in which 10 and 20 μL mL^{-1} concentrations were taken for the Ag NPs, Ag NPs−PANI, and Ag NPs−PANI/MWCNT nanocomposites. Indeed, the comparative study of discs with standard drug streptomycin and penicillin was also carried out. Then, the zone of inhibition was measured after 24 h of incubation at 37 °C of the *E. coli* and *S. aureus* bacteria at a different concentration of the catalyst as shown in Table 1. The Ag NPs−PANI/MWCNT nanocomposites have shown that 20 and 19 mm zones of inhibition at 20 μL mL^{-1} were higher than Ag NP and Ag NPs−PANI catalysts at the same concentration for the *E. coli* and *S. aureus* bacteria, respectively, as shown in Figure 8. The well dispersion, proper interconnectivity between the component and overall stability of the NCs are mainly responsible for the enhanced bacterial inactivation of the bacteria. In addition, it is also seen that the inactivation are of *E. coli* bacteria using NCs is somewhat higher to that of *S.aureus* bacteria because of the thinner wall of *E. coli* bacteria. In all cases, 20 μL mL^{-1} is a higher zone of inhibition because of the higher silver concentration, and it is more efficient on Gram-negative bacteria than Gram-positive bacteria. Silver is used in a broad spectrum as a biocide agent, having a plausible mechanism dependent on the different

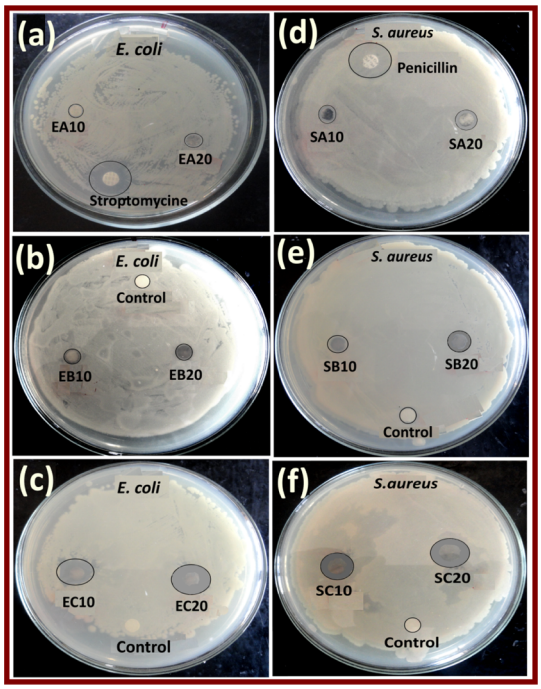

Figure 8. Zone of inhibition observed of *E. coli* (a) Ag NPs, (b) Ag NPs−PANI, and (c) Ag NPs−PANI/MWCNTs and *S. aureus* (d) Ag NPs, (e) Ag NPs−PANI, and (f) Ag NPs PANI/MWCNT bacteria at 10 and 20 μL mL^{-1} of the nanocomposites.

parameters such as (i) dimension and character of NPs or (ii) physicochemical interaction between the donor atoms as N, S, and O of bacteria with its cation. Subsequently, bacterial respiration and adenosine triphosphate syntheses are disturbing because of the silver ions attached to the DNA of bacteria.[46] However, the zone of inhibition of reference drugs streptomycin and penicillin 20 and 22 mm was observed that is comparable with our Ag NPs−PANI/MWCNT nanocomposites. These results which were comparable with Co−PANI/MWCNT nanocomposites are reported in the literature.[47] The well dispersion of NCs results into higher surface area of Ag NPs and acidic functional group of PANI led to bacterial inactivation.[48] It also showed higher antibacterial enforcement to the Gram-negative cell wall, having reduced the osmotic pressure that maintains the physical interaction between them.[49,50] In addition, the various chemical factors of PANI such as surface hydrophilicity, polymer chain length, and molecular weight are responsible for the enhanced permeability of the bacterial cell membrane and development of stress-resistant bio-films.[51] MWCNTs also exhibit antibacterial activity because their 1D nanomaterials form composites with zero-dimensional silver nanoparticles, which enhances the

DOI: 10.1021/acsomega.9b02526
ACS Omega 2020, 5, 219−227

physical property of silver nanoparticles for antibacterial application.[16] Nevertheless, the charged functionalities have enhanced interactions with the surface of bacteria. It leads to penetration into the cell with higher permeability with the membrane, decrease in metabolic function, and finally cell death.[52] As a result, we show that ternary hybrid Ag NPs−PANI/MWCNTs have not only an active catalyst against the 4-NP pollutant but also effective biocides against both types of bacteria.

3. CONCLUSIONS

Metal-supported PANI/MWCNT was synthesized using the in situ polymerization of aniline for effective catalysis and antibacterial application. The spectroscopic and instrumental techniques have revealed its chemical and structural properties. The apparent rate of reaction (K_{app}) for reduction 4-NP to 4-AP is $K_1 = 5.4 \times 10^{-3}$ s^{-1} and $K_2 = 3.9 \times 10^{-3}$ s^{-1} for Ag NPs−PANI/MWCNTs and Ag NPs−PANI, respectively. The rate constant reveals that the Ag NPs−PANI/MWCNTs have enhanced the rate of reaction as compared to Ag NPs−PANI nanocomposites. The conducting support material and higher adsorption of the reactant on the catalyst led to significant catalytic activities. The antibacterial study reveals that ternary nanocomposites are in the higher zone of inhibition as compared to binary nanocomposites. The synergistic effect of nanocomposites makes them a more effective antibacterial agent against Gram-negative and Gram-positive bacteria. Therefore, such a type of hybrid ternary nanocomposites has been explored for use in the field of catalysis as well as biomedical sectors.

4. EXPERIMENTAL SECTION

4.1. Materials. The monomer, aniline, was purchased from Thomas Baker India, and ammonium persulphate [$(NH_4)_2S_2O_8$], sodium dodecyl sulfate, and silver nitrate ($AgNO_3$) were purchased from Qualigenes, India. MWCNTs were obtained from Nanotechnology India. These MWCNTs had a length of 20 μm, a diameter of 10−20 nm, and aspect ratios of 1000. Double distilled water was used during the synthesis.

4.2. Synthesis of Ag NPs−PANI Nanocomposites. The synthesis of the Ag−PANI nanocomposite was carried out using the in situ polymerization method. In a round-bottom flask, 10 mL of 0.01 M silver nitrate solution was stirred for 30 min, and dextrose (10 mL, 10 mM) was added with stirring in the flat bottom flask. Then, 0.1 M of 20 mL of sodium dodecyl sulphate solution was added with constant stirring. Then, precooled 0.5 mL of aniline solution, 1.26 g mL^{-1} of *p*-TSA, and 0.01 M of ammonium persulphate were added dropwise and constantly stirred for 12 h. The Ag−PANI nanocomposite was filtered and washed with alcohol and dried in the oven for 2 h. The Ag NPs−PANI nanocomposite was filtered and washed with alcohol and dried in the oven for 2 h.

4.3. Synthesis of Ag NPs−PANI/MWCNT Nanocomposites. Ternary nanocomposites of Ag NPs−PANI/MWCNTs have been synthesized with a typical, in situ chemical method. F-MWCNTs (60 mg) were added in aqueous solution and sonicated for 45 min at room temperature. In another round-bottom flask, silver nitrate was stirred for 20 min at room temperature, and the sodium dodecyl sulphate solution was added. Then, the dextrose solution was added with constant stirring. Afterward, 0.5 mL of the aniline monomer and *p*-TSA was added, followed by addition of ammonium persulphate dropwise for the polymerization of aniline. The aspect ratio (1:1) of the monomer and the oxidizing agent was maintained during the reaction. Then, dispersed solution of MWCNTs was added and stirred for 15 min. The whole reaction mixture was stirred for 12 h for complete polymerization of aniline. Consequently, the final product was dried at 70 °C to acquire nanocomposites. Scheme 1 represents the synthetic protocol of Ag NPs−PANI/MWCNT nanocomposites.

Scheme 1. Schematic Illustration of Ag NPs−PANI/MWCNT Nanocomposites

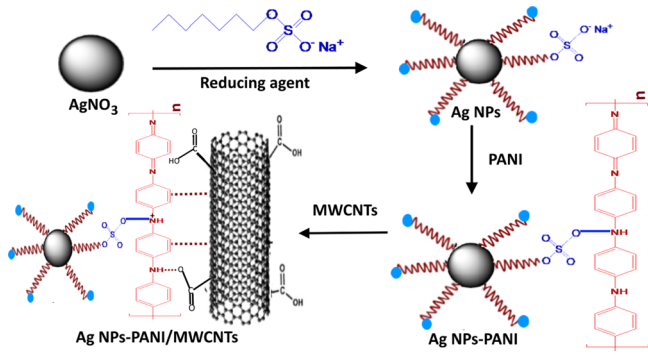

4.4. Catalytic Reduction of 4-NP. The catalytic activity of Ag NPs−PANI/MWCNTs and Ag NPs−PANI was studied for the reduction of 4-NP to 4-AP using $NaBH_4$ as a reducing agent at room temperature. In this case, aqueous solution of 4-NP [$(1 \times 10^{-4}$ M), 0.2 mL] was taken in the cuvette, and [0.1 M, 2 mL] $NaBH_4$ was added in the cuvette. Afterward, Ag NPs−PANI/MWCNTs and Ag NPs−PANI nanocomposites (1 mg) were added. Subsequently, the change in the concentration of 4-NP was monitored using a UV−visible spectrometer.

4.5. Antibacterial Study. The antibacterial study of Ag NPs, Ag NPs−PANI, and Ag NPs−PANI/MWCNTs was carried out by the disc diffusion method and broth macrodilution method. The human pathogenic bacteria strain of *S. aureus* and *E. coli* was used for the study. The disc diffusion method was used for the determination of antibacterial efficacy; the bacteria were grown 24 h in the liquid nutrient broth. Then, a laminar air flow-sterilized Mueller Hinton agar medium was transferred into autoclaved Petri dishes. After the medium solidified, the culture of each bacterium was uniformly spread on the surface using a glass spreader. In each Petri dish, sterile paper discs impregnated with 10−20 μL each of Ag NPs, Ag NPs−PANI, and Ag NPs−PANI/MWCNT nanocomposites were inoculated and then incubated at 37 °C for 24 h. Then, the zone of inhibition was measured in millimeter (mm). The comparative studies have been carried with Ag NPs−PANI/MWCNT nanocomposites in the presence of standard drugs such as streptomycin and penicillin. All the experiments were performed in triplicates.

4.6. Characterizations. UV−visible spectra of nanocomposites were analyzed with a UV−VIS 3092 spectrophotometer having a wavelength range of 200−800 nm, which was obtained from Lab India. FTIR spectra of samples were used to determine the functional group as well as chemical constitutes of the composites recorded in the range of 500−4000 cm^{-1} using the FTIR Thermo Fisher India instrument. XRD analysis

DOI: 10.1021/acsomega.9b02526
ACS Omega 2020, 5, 219−227

of Ag NPs−PANI/MWCNTs was carried out by a PerkinElmer PHI-5400 diffractometer, employing Cu Kα radiation of wavelength 1.5406 Å. The data were taken in the range of 10−90° (2θ), with a step size of 0.02°. The TEM (JEM-2100) model was used for the morphology and particle size analysis. Raman spectra of the sample were observed by using a FT-Raman spectrophotometer (Bruker MultiRAM, Germany make) in the spectral range of 1000−1800 cm^{-1}. Chemical status and its bonding were determined by XPS, VG Multilab 2000, Thermo VG Scientific, UK with a monochromatic Mg Kα (1253.6 eV) radiation source.

■ ASSOCIATED CONTENT

Supporting Information

The Supporting Information is available free of charge at https://pubs.acs.org/doi/10.1021/acsomega.9b02526.

Experimental section, materials, modification of MWCNTs, synthesis of PANI, UV−visible spectra of F-MWCNTs and PANI, XRD pattern of PANI, TEM images of F-MWCNTs, PANI, particle size histogram of PANI, particle size histogram of Ag NPs−PANI, and particle size histogram of Ag NPs−PANI/MWCNTs, scanning electron micrographs of Ag NPs−PANI and Ag NPs−PANI/MWNCNTs, and Raman spectra of PANI (PDF)

■ AUTHOR INFORMATION

Corresponding Author

*E-mail: sddelekar7@rediffmail.com.

ORCID

Sagar D. Delekar: 0000-0002-4510-305X

Notes

The authors declare no competing financial interest.

■ ACKNOWLEDGMENTS

The authors would like to thankful University Grants Commission, New Delhi, for financial assistance under the FDP scheme [UGC-F. no.—38-11/15 (WRO) Pune] which is gratefully acknowledged.

■ REFERENCES

(1) Tong, H.; Ouyang, S.; Bi, Y.; Umezawa, N.; Oshikiri, M.; Ye, J. Nano-photocatalytic materials: possibilities and challenges. *Adv. Mater.* **2012**, *24*, 229−251.

(2) Deshmukh, S. P.; Patil, S. M.; Mullani, S. B.; Delekar, S. D. Silver nanoparticles as an effective disinfectant: A review. *Mater. Sci. Eng., C* **2019**, *97*, 954−965.

(3) Patil, S. M.; Deshmukh, S. P.; Dhodamani, A. G.; More, K. V.; Delekar, S. D. Different Strategies for Modification of Titanium Dioxide as Heterogeneous Catalyst in Chemical Transformations. *Curr. Org. Chem.* **2017**, *21*, 821−833.

(4) Xiao, W.; Zhang, Y.; Liu, B. Raspberrylike SiO_2@Reduced Graphene Oxide@AgNP Composite Microspheres with High Aqueous Dispersity and Excellent Catalytic Activity. *ACS Appl. Mater. Interfaces* **2015**, *7*, 6041−6046.

(5) Kuroda, K.; Ishida, T.; Haruta, M. Reduction of 4-nitrophenol to 4-aminophenol over Au nanoparticles deposited on PMMA. *J. Mol. Catal. A: Chem.* **2009**, *298*, 7−11.

(6) Zhang, Y.; Liu, S.; Lu, W.; Wang, L.; Tian, J.; Sun, X. In situ green synthesis of Au nanostructures on graphene oxide and their application for catalytic reduction of 4-nitrophenol. *Catal. Sci. Technol.* **2011**, *1*, 1142−1144.

(7) Jiang, Z.-J.; Liu, C.-Y.; Sun, L.-W. Catalytic properties of silver nanoparticles supported on silica spheres. *J. Phys. Chem. B* **2005**, *109*, 1730−1735.

(8) He, J.; Razzaque, S.; Jin, S.; Hussain, I.; Tan, B. Efficient Synthesis of Ultrafine Gold Nanoparticles with Tunable Sizes in a Hyper-Cross-Linked Polymer for Nitrophenol Reduction. *ACS Appl. Nano Mater.* **2019**, *2*, 546−553.

(9) Li, C.; Thostenson, E. T.; Chou, T.-W. Sensors and actuators based on carbon nanotubes and their composites: a review. *Compos. Sci. Technol.* **2008**, *68*, 1227−1249.

(10) Palaniappan, S.; John, A. Polyaniline materials by emulsion polymerization pathway. *Prog. Polym. Sci.* **2008**, *33*, 732−758.

(11) Shaban, M.; Rabia, M.; Fathallah, W.; El-Mawgoud, N. A.; Mahmoud, A.; Hussien, H.; Said, O. Preparation and characterization of polyaniline and Ag/polyaniline composite nanoporous particles and their antimicrobial activities. *J. Polym. Environ.* **2018**, *26*, 434−442.

(12) Tamboli, M. S.; Kulkarni, M. V.; Patil, R. H.; Gade, W. N.; Navale, S. C.; Kale, B. B. Nanowires of silver−polyaniline nanocomposite synthesized via in situ polymerization and its novel functionality as an antibacterial agent. *Colloids Surf., B* **2012**, *92*, 35−41.

(13) Yuan, C.; Yiting, X.; Lina, Z.; Long, Z.; Cangjie, Y.; Binjie, J.; Yuanming, D.; Birong, Z.; Ning, H.; Weiang, L.; Lizong, D. Heterogeneous silver−polyaniline nanocomposites with tunable morphology and controllable catalytic properties. *Nanotechnology* **2013**, *24*, 185602.

(14) Barkade, S. S.; Naik, J. B.; Sonawane, S. H. Ultrasound assisted miniemulsion synthesis of polyaniline/Ag nanocomposite and its application for ethanol vapor sensing. *Colloids Surf., A* **2011**, *378*, 94−98.

(15) Delekar, S. D.; Dhodamani, A. G.; More, K. V.; Dongale, T. D.; Kamat, R. K.; Acquah, S. F. A.; Dalal, N. S.; Panda, D. K. Structural and Optical Properties of Nanocrystalline TiO_2 with Multiwalled Carbon Nanotubes and Its Photovoltaic Studies Using Ru(II) Sensitizers. *ACS Omega* **2018**, *3*, 2743−2756.

(16) Niu, A.; Han, Y.; Wu, J.; Yu, N.; Xu, Q. Synthesis of one-dimensional carbon nanomaterials wrapped by silver nanoparticles and their antibacterial behavior. *J. Phys. Chem. C* **2010**, *114*, 12728−12735.

(17) Wen, J.; Tan, X.; Hu, Y.; Guo, Q.; Hong, X. Filtration and Electrochemical Disinfection Performance of PAN/PANI/AgNWs-CC Composite Nanofiber Membrane. *Environ. Sci. Technol.* **2017**, *51*, 6395−6403.

(18) Hussein, M. A.; El-Shishtawy, R. M.; Alamry, K. A.; Asiri, A. M.; Mohamed, S. A. Efficient water disinfection using hybrid polyaniline/graphene/carbon nanotube nanocomposites. *Environ. Technol.* **2019**, *40*, 2813.

(19) Zhang, P.; Shao, C.; Zhang, Z.; Zhang, M.; Mu, J.; Guo, Z.; Liu, Y. In situ assembly of well-dispersed Ag nanoparticles (AgNPs) on electrospun carbon nanofibers (CNFs) for catalytic reduction of 4-nitrophenol. *Nanoscale* **2011**, *3*, 3357−3363.

(20) Wang, Z.; Xu, C.; Li, X.; Liu, Z. In situ green synthesis of Ag nanoparticles on tea polyphenols-modified graphene and their catalytic reduction activity of 4-nitrophenol. *Colloids Surf., A* **2015**, *485*, 102−110.

(21) Qiao, X.; Liu, X.; Li, X.; Xing, S. Anchoring gold nanoparticles inside polyaniline shells with magnetic cores for the enhancement of catalytic stability. *New J. Chem.* **2015**, *39*, 8588−8593.

(22) Ayad, M. M.; Amer, W. A.; Kotp, M. G.; Minisy, I. M.; Rehab, A. F.; Kopecký, D.; Fitl, P. Synthesis of silver-anchored polyaniline−chitosan magnetic nanocomposite: a smart system for catalysis. *RSC Adv.* **2017**, *7*, 18553−18560.

(23) Karim, M. R.; Lim, K. T.; Lee, C. J.; Bhuiyan, M. T. I.; Kim, H. J.; Park, L.-S.; Lee, M. S. Synthesis of core-shell silver−polyaniline nanocomposites by gamma radiolysis method. *J. Polym. Sci., Part A: Polym. Chem.* **2007**, *45*, 5741−5747.

(24) Choudhury, A. Polyaniline/silver nanocomposites: Dielectric properties and ethanol vapour sensitivity. *Sens. Actuators, B* **2009**, *138*, 318−325.

DOI: 10.1021/acsomega.9b02526
ACS Omega 2020, 5, 219−227

(25) Reddy, K. R.; Sin, B. C.; Ryu, K. S.; Kim, J.-C.; Chung, H.; Lee, Y. Conducting polymer functionalized multi-walled carbon nanotubes with noble metal nanoparticles: synthesis, morphological characteristics and electrical properties. *Synth. Met.* **2009**, *159*, 595−603.
(26) Li, Z.; Li, Y.; Lin, W.; Zheng, F.; Laven, J. Polyaniline/silver nanocomposites synthesized via UV−Vis-assisted aniline polymerization with a reversed micellar microemulsion system. *Polym. Compos.* **2016**, *37*, 1064−1071.
(27) Kshirsagar, A. S.; Hiragond, C.; Dey, A.; More, P. V.; Khanna, P. K. Band Engineered I/III/V−VI Binary Metal Selenide/MWCNT/PANI Nanocomposites for Potential Room Temperature Thermoelectric Applications. *ACS Appl. Energy Mater.* **2019**, *2*, 2680−2691.
(28) Grinou, A.; Bak, H.; Yun, Y. S.; Jin, H.-J. Polyaniline/silver nanoparticle-doped multiwalled carbon nanotube composites. *J. Dispersion Sci. Technol.* **2012**, *33*, 750−755.
(29) Yan, J.; Wei, T.; Shao, B.; Fan, Z.; Qian, W.; Zhang, M.; Wei, F. Preparation of a graphene nanosheet/polyaniline composite with high specific capacitance. *Carbon* **2010**, *48*, 487−493.
(30) Tamboli, M. S.; Kulkarni, M. V.; Deshmukh, S. P.; Kale, B. B. Synthesis and spectroscopic characterisation of silver−polyaniline nanocomposite. *Mater. Res. Innovations* **2013**, *17*, 112−116.
(31) Saleh, T. A. The influence of treatment temperature on the acidity of MWCNT oxidized by HNO_3 or a mixture of HNO_3/H_2SO_4. *Appl. Surf. Sci.* **2011**, *257*, 7746−7751.
(32) Dhibar, S.; Das, C. K. Silver nanoparticles decorated polyaniline/multiwalled carbon nanotubes nanocomposite for high-performance supercapacitor electrode. *Ind. Eng. Chem. Res.* **2014**, *53*, 3495−3508.
(33) Yan, X. B.; Han, Z. J.; Yang, Y.; Tay, B. K. NO_2 gas sensing with polyaniline nanofibers synthesized by a facile aqueous/organic interfacial polymerization. *Sens. Actuators, B* **2007**, *123*, 107−113.
(34) Grover, S.; Goel, S.; Sahu, V.; Singh, G.; Sharma, R. K. Asymmetric Supercapacitive Characteristics of PANI Embedded Holey Graphene Nanoribbons. *ACS Sustainable Chem. Eng.* **2015**, *3*, 1460−1469.
(35) Patil, D. S.; Shaikh, J. S.; Pawar, S. A.; Devan, R. S.; Ma, Y. R.; Moholkar, A. V.; Kim, J. H.; Kalubarme, R. S.; Park, C. J.; Patil, P. S. Investigations on silver/polyaniline electrodes for electrochemical supercapacitors. *Phys. Chem. Chem. Phys.* **2012**, *14*, 11886−11895.
(36) Zhou, Y.-k.; He, B.-l.; Zhou, W.-j.; Li, H.-l. Preparation and electrochemistry of SWNT/PANI composite films for electrochemical capacitors. *J. Electrochem. Soc.* **2004**, *151*, A1052−A1057.
(37) Nguyen, V. H.; Shim, J. J. Green synthesis and characterization of carbon nanotubes/polyaniline nanocomposites. *J. Spectrosc.* **2015**, *2015*, 297804.
(38) Shi, L.; Liang, R.-P.; Qiu, J.-D. Controllable deposition of platinum nanoparticles on polyaniline-functionalized carbon nanotubes. *J. Mater. Chem.* **2012**, *22*, 17196−17203.
(39) Deshmukh, S. P.; Dhokale, R. K.; Yadav, H. M.; Achary, S. N.; Delekar, S. D. Titania−supported silver nanoparticles: An efficient and reusable catalyst for reduction of 4-nitrophenol. *Appl. Surf. Sci.* **2013**, *273*, 676−683.
(40) Tian, G.; Wang, W.; Mu, B.; Kang, Y.; Wang, A. Ag (I)-triggered one-pot synthesis of Ag nanoparticles onto natural nanorods as a multifunctional nanocomposite for efficient catalysis and adsorption. *J. Colloid Interface Sci.* **2016**, *473*, 84−92.
(41) Chang, G.; Luo, Y.; Lu, W.; Qin, X.; Asiri, A. M.; Al-Youbi, A. O.; Sun, X. Ag nanoparticles decorated polyaniline nanofibers: synthesis, characterization, and applications toward catalytic reduction of 4-nitrophenol and electrochemical detection of H_2O_2 and glucose. *Catal. Sci. Technol.* **2012**, *2*, 800−806.
(42) Xu, W.; Kong, J. S.; Yeh, Y.-T. E.; Chen, P. Single-molecule nanocatalysis reveals heterogeneous reaction pathways and catalytic dynamics. *Nat. Mater.* **2008**, *7*, 992.
(43) Ma, B.; Wang, M.; Tian, D.; Pei, Y.; Yuan, L. Micro/nano-structured polyaniline/silver catalyzed borohydride reduction of 4-nitrophenol. *RSC Adv.* **2015**, *5*, 41639−41645.
(44) Cao, J.; Mei, S.; Jia, H.; Ott, A.; Ballauff, M.; Lu, Y. In Situ Synthesis of Catalytic Active Au Nanoparticles onto Gibbsite−Polydopamine Core−Shell Nanoplates. *Langmuir* **2015**, *31*, 9483−9491.
(45) Banerjee, M.; Sharma, S.; Chattopadhyay, A.; Ghosh, S. S. Enhanced antibacterial activity of bimetallic gold-silver core−shell nanoparticles at low silver concentration. *Nanoscale* **2011**, *3*, 5120−5125.
(46) Dallas, P.; Sharma, V. K.; Zboril, R. Silver polymeric nanocomposites as advanced antimicrobial agents: classification, synthetic paths, applications, and perspectives. *Adv. Colloid Interface Sci.* **2011**, *166*, 119−135.
(47) Bushra, R.; Arfin, T.; Oves, M.; Raza, W.; Mohammad, F.; Khan, M. A.; Ahmad, A.; Azam, A.; Muneer, M. Development of PANI/MWCNTs decorated with cobalt oxide nanoparticles towards multiple electrochemical, photocatalytic and biomedical application sites. *New J. Chem.* **2016**, *40*, 9448−9459.
(48) Agarwala, M.; Barman, T.; Gogoi, D.; Choudhury, B.; Pal, A. R.; Yadav, R. N. S. Highly effective antibiofilm coating of silver−polymer nanocomposite on polymeric medical devices deposited by one step plasma process. *J. Biomed. Mater. Res., Part B* **2014**, *102*, 1223−1235.
(49) Jia, Q.; Shan, S.; Jiang, L.; Wang, Y.; Li, D. Synergistic antimicrobial effects of polyaniline combined with silver nanoparticles. *J. Appl. Polym. Sci.* **2012**, *125*, 3560−3566.
(50) Deshmukh, S. P.; Mullani, S. B.; Koli, V. B.; Patil, S. M.; Kasabe, P. J.; Dandge, P. B.; Pawar, S. A.; Delekar, S. D. Ag Nanoparticles Connected to the Surface of TiO_2 Electrostatically for Antibacterial Photoinactivation Studies. *Photochem. Photobiol.* **2018**, *94*, 1249−1262.
(51) Poyraz, S.; Cerkez, I.; Huang, T. S.; Liu, Z.; Kang, L.; Luo, J.; Zhang, X. One-step synthesis and characterization of polyaniline nanofiber/silver nanoparticle composite networks as antibacterial agents. *ACS Appl. Mater. Interfaces* **2014**, *6*, 20025−20034.
(52) Mohan, R.; Shanmugharaj, A. M.; Sung Hun, R. An efficient growth of silver and copper nanoparticles on multiwalled carbon nanotube with enhanced antimicrobial activity. *J. Biomed. Mater. Res., Part B* **2011**, *96B*, 119−126.

NOTE ADDED AFTER ASAP PUBLICATION

This paper was published ASAP on December 26, 2019, with an incorrect Figure 5. The corrected version was reposted on December 27, 2019.

DOI: 10.1021/acsomega.9b02526
ACS Omega 2020, 5, 219−227